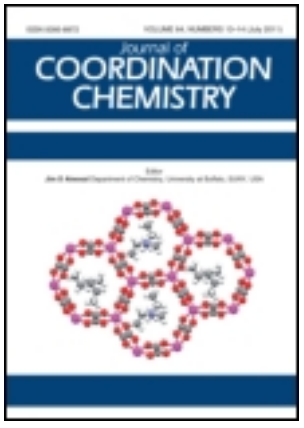

Journal of Coordination Chemistry
Publication details, including instructions for authors and subscription information:
http://www.tandfonline.com/loi/gcoo20

Ruthenium(II) complexes: structure, DNA-binding, photocleavage, antioxidant activity, and theoretical studies

Xian-Lan Hong [a] , Zhen-Hua Liang [b] & Mao-Hua Zeng [a]
[a] Department of Chemistry , Shaoguan University , Shaoguan, Guangdong 512005, P.R. China
[b] School of Pharmacy , Guangdong Pharmaceutical University , Guangzhou 510006, P.R. China
Published online: 04 Nov 2011.

To cite this article: Xian-Lan Hong , Zhen-Hua Liang & Mao-Hua Zeng (2011) Ruthenium(II) complexes: structure, DNA-binding, photocleavage, antioxidant activity, and theoretical studies, Journal of Coordination Chemistry, 64:21, 3792-3807, DOI: 10.1080/00958972.2011.628989

To link to this article: http://dx.doi.org/10.1080/00958972.2011.628989

Journal of Coordination Chemistry
Vol. 64, No. 21, 10 November 2011, 3792–3807

Ruthenium(II) complexes: structure, DNA-binding, photocleavage, antioxidant activity, and theoretical studies

XIAN-LAN HONG*†, ZHEN-HUA LIANG‡ and MAO-HUA ZENG†

†Department of Chemistry, Shaoguan University, Shaoguan, Guangdong 512005, P.R. China
‡School of Pharmacy, Guangdong Pharmaceutical University, Guangzhou 510006, P.R. China

(*Received 19 May 2011; in final form 8 September 2011*)

Two triazine-containing ruthenium(II) complexes, $[Ru(dmb)_2(pdpt)](ClO_4)_2$ (dmb = 4,4′-dimethyl-2,2′-bipyridine, pdpt = 3-(pyridine-2-yl)-5,6-diphenyl-as-triazine) (**1**) and $[Ru(dmb)_2(pdtp)](ClO_4)_2$ (pdtp = 3-(pyridine-2-yl)-as-triazino[5,6-f]phenanthrene) (**2**), were synthesized and characterized by elemental analysis, ES-MS, ^{1}H NMR, UV-Vis spectra, and cyclic voltammetry; the crystal structure of **2** was determined by X-ray diffraction. DNA-binding behaviors of both complexes were studied by absorption titration, thermal denaturation, and viscosity measurements. The photoactivated DNA cleavage of plasmid pBR322 in the presence of **1** and **2** was explored through gel electrophoresis. Antioxidant activities of the two complexes against hydroxyl radical (·OH) were also investigated. The results indicate that the DNA-binding affinity of **2** is much greater than that of **1**, and that **2** binds to calf thymus DNA by intercalation, but **1** binds in partial intercalation, with π–π stacking on the DNA surface. Experimental findings made through analysis of the CV, absorption spectra, X-ray crystal structure, and the DNA-binding properties were compared with those of theoretical studies using density functional calculations.

Keywords: Ruthenium complex; DNA-binding; DNA-photocleavage; Antioxidant activity

1. Introduction

It has been two decades since the initial, thought-provoking research on the interaction of Ru(II)-polypyridyl complexes with DNA was published [1, 2]. A series of significant results and methods to broaden this research area have been reviewed [3–5]. Ruthenium complexes have applications in biotechnology and synthetic pharmacology as DNA-binding or DNA-probing agents [6–9], and as a component of chemical antic-arcinogenic drugs [10], based on their special molecular structures and unique photophysical, photochemical, and electrochemical properties [11]. Clinical cancer therapeutic drugs, such as cisplatin [12] and some Ru(III) chloride complexes [10, 13], generally act by covalently binding to DNA in cancer cells, inhibiting the division of cancer cells and resulting in cell death. By contrast, ruthenium(II) polypyridyl

*Corresponding author. Email: hongxianlan@yahoo.com.cn

ISSN 0095-8972 print/ISSN 1029-0389 online
http://dx.doi.org/10.1080/00958972.2011.628989

complexes are coordinatively saturated and substitutionally inert, but can noncovalently interact with double helix DNA through intercalation, groove-binding, and electrostatic attraction. Such interactions, especially intercalations, have recently been verified as capable of causing DNA photo-induced damage in cancer cells, and thus also possess anticancer activity [14–17].

In the process of exploring polypyridyl ruthenium(II) complexes as DNA agents and an alternative anticancer drug to the platinum complex, the key issue has proven to be the synthesis of Ru(II) compounds with large DNA-binding affinities and can deeply insert DNA base pairs [15, 17]. Triazine rings containing pdpt and pdtp were chosen, as the main ligands and dmb as the auxiliary ligand, to construct Ru(II) complexes **1** and **2** (figure 1). The triazine ring has an energetically low-lying LUMO, facilitating receiving of electron density from DNA base pairs as it inserts into the DNA double helix [18, 19].

In order to systematically study the structure, DNA-binding properties, DNA-photocleavage properties, and antioxidant activities of **1** and **2**, a series of experiments involving X-ray single-crystal diffraction, electronic absorption titration, thermal denaturation, viscosity determination, and gel electrophoresis were carried out. Density functional theory was used *via* the density functional calculation (DFT)/B3LYP method in an attempt to correlate experimental findings with theoretical predictions [20, 21]. The experimental results agree with theoretical data. These results will play an important role in guiding the development of strong DNA-intercalators. In addition, the antioxidant activity on hydroxyl radical showed **1** and **2** may have potential as antioxidants.

2. Experimental

2.1. *General*

The ligands pdpt and pdtp [22] and the precursor *cis*-[Ru(dmb)$_2$Cl$_2$] [23] were synthesized according to literature methods. Calf thymus DNA (CT-DNA;

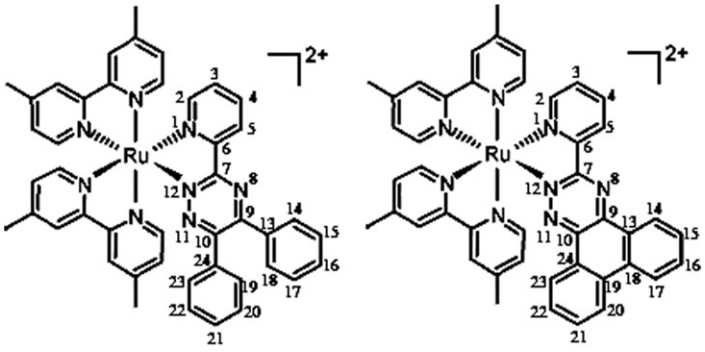

Figure 1. Structures of **1** (left) and **2** (right) with atom-numbering scheme for theoretical calculation.

Sigma Chemical Co.), pBR 322 DNA (Shanghai Sangon Biological Engineering & Services Co.), agarose, ethidium bromide (EB) (Aldrich), and other chemicals were commercially available. Buffer A (5 mmol L^{-1} Tris-HCl, 50 mmol L^{-1} NaCl, pH 7.0) was used for absorption titration, viscosity measurements, and equilibrium dialyses. Buffer B (50 mmol L^{-1} Tris-HCl, 18 mmol L^{-1} NaCl, pH 7.2) was used for DNA photocleavage experiments and Buffer C (1.5 mmol L^{-1} Na_2HPO_4, 0.5 mmol L^{-1} NaH_2PO_4, 0.25 mmol L^{-1} Na_2EDTA, pH 7.0) was used for thermal DNA denaturation experiments. A solution of CT-DNA in Buffer A gave a ratio of UV absorbance at 260 and 280 nm of *ca* 1.8–1.9 : 1, indicating that the DNA was sufficiently free of protein [24]. The DNA concentration per nucleotide was determined with the spectrophotometric method by assuming $\varepsilon_{260} = 6600$ mol L^{-1} cm^{-1} at 260 nm [25].

Microanalyses (C, H, and N) were carried out on a Perkin-Elmer 240Q elemental analyzer. Absorption spectra were recorded with a Perkin-Elmer Lambda 35 spectrophotometer, ^{1}H NMR spectra were measured on Varian INOVA-500 spectrometers with $(CD_3)_2SO$ as solvent at room temperature and TMS as the internal standard. Electrospray mass spectra (ES-MS) were recorded on an LQC system (Finnigan MAT, USA) using CH_3CN as the mobile phase, and the quoted *m*/*z* values are for the major peaks in the isotope distribution.

A Bioanalytical Systems 100-W electrochemical analyzer was used to record the cyclic voltammograms. The supporting electrolyte was 0.1 mol L^{-1} tetrabutylammonium perchlorate in acetonitrile, freshly distilled from phosphorus pentaoxide and deaerated through purging with nitrogen. The electrochemical measurements were made in a standard three-electrode system using a platinum disc working electrode, platinum-wire auxiliary electrode and a Ag/AgCl reference electrode [0.29 V *vs*. NHE, calibrated using the $Fe(C_5H_5)_2/Fe(C_5H_5)_2^+$ couple (0.665 V *vs*. NHE)]. All cyclic voltammograms were recorded at a scan rate of 200 mV s^{-1}.

2.2. *Chemical synthesis*

2.2.1. [Ru(dmb)$_2$(pdpt)](ClO$_4$)$_2$ · H$_2$O (1). A mixture of $Ru(dmb)_2Cl_2 \cdot 2H_2O$ (0.144 g, 0.25 mmol) and pdpt (0.078 g, 0.25 mmol) in 20 cm^3 ethanol–water (v/v, 3 : 1) was refluxed under Ar for 8 h, with vigorous magnetic stirring maintained throughout the process. After being cooled to ambient temperature, the ethanol was removed under reduced pressure and a saturated solution of aqueous $NaClO_4$ was added to obtain a red-brown precipitate, which was then purified on a neutral alumina column with acetonitrile–toluene (v/v, 2 : 1) as eluant. Yield: 70%. ^{1}H NMR [$(CD_3)_2SO$]: δ 8.84 (d, 1H, $J = 7.5$), 8.77 (s, 1H), 8.72 (s, 1H), 8.60 (s, 2H), 8.24 (t, 2H, $J_1 = 8$, $J_2 = 7.5$), 8.05 (d, 1H, $J_1 = 6$), 7.95 (d, H, $J = 5$), 7.72 (m, 5H), 7.54 (m, 2H), 7.47 (m, 4H), 7.33 (m, 4H), 7.10 (dd, 2H, $J_1 = 8.5$, $J_2 = 8.5$), 2.57 (s, 3H), 2.55 (s, 3H), 2.53 (s, 3H), 2.50 (s, 3H). ES-MS (CH_3CN): *m*/*z* 879.00 ($[M-ClO_4]^+$) and 390.27 ($[M-2ClO_4]^{2+}$). Anal. Calcd for $C_{44}H_{38}N_8Cl_2O_8Ru$ (%): C, 53.99; H, 3.91; N, 11.45. Found (%): C, 54.10; H, 3.98; N, 11.77.

2.2.2. [Ru(dmb)$_2$(pdtp)](ClO$_4$)$_2$ · H$_2$O (2). This complex (dark brown) was synthesized in a method identical to the one described for **1**, except pdtp (0.077 g, 0.25 mmol) replaced pdpt. Yield: 74%. ^{1}H NMR [$(CD_3)_2SO$]: δ 9.44 (dd, 1H, $J_1 = 8.5$, $J_2 = 8$),

9.15 (d, 1H, $J=7$), 8.87 (t, 2H, $J_1=9.5$, $J_2=8.5$), 8.81 (s, 1H), 8.74 (d, 2H, $J=11.5$), 8.62 (s, 1H), 8.30 (t, 1H, $J_1=7.5$, $J_2=8$), 8.07 (t, 1H, $J_1=8.5$, $J_2=8$), 7.99 (m, 3H), 7.94 (t, 2H, $J_1=8.5$, $J_2=7$), 7.78 (m, 3H), 7.70 (t, 1H, $J_1=7$, $J_2=8.5$), 7.61 (d, 1H, $J=6$), 7.50 (t, 2H, $J_1=4.5$, $J_2=5.5$), 7.36 (d, 1H, $J=4.5$), 7.21 (d, 1H, $J=5$), 2.68 (s, 3H), 2.59 (s, 3H), 2.51 (s, 3H), 2.44 (s, 3H). ES-MS (CH_3CN): m/z 877.00 ($[M-ClO_4]^+$) and 389.27 ($[M-2ClO_4]^{2+}$). Anal. Calcd for $C_{44}H_{36}N_8Cl_2O_8Ru$ (%): C, 54.10; H, 3.71; N, 11.47. Found (%): C, 54.63; H, 3.79; N, 11.53.

Caution: Perchlorate complexes are potential explosives that must be handled in small quantities and with great care.

2.3. *X-ray crystallography*

The crystal of **2** suitable for X-ray single-crystal analysis was obtained through slow evaporation of acetonitrile–toluene (1 : 1, v/v) solution at ambient temperature. Diffraction data were collected on a Bruker Smart 1000 CCD diffractometer equipped with graphite monochromated Mo-Kα radiation ($\lambda=0.71073$ Å) at 100 K. Absorption corrections for **2** were applied by SADABS [26]. The structure was solved by direct methods and refined using full-matrix least-squares/difference Fourier techniques using SHELXTL [27, 28]. All non-hydrogen atoms were refined with anisotropic displacement parameters. All hydrogen atoms of the ligands were placed at idealized positions and refined as riding atoms with the relative isotropic parameters of the heavy atoms to which they are attached.

2.4. *DNA-binding and photoactivated cleavage*

The DNA-binding and photoactivated cleavage experiments were performed at room temperature. Absorption titration of the ruthenium(II) complex in buffer was carried out using a fixed concentration of **1** or **2** solution to which increments of the DNA stock solution were added. 10 μmol L^{-1} Ru(II)-solution was employed and CT-DNA was added to a 10 : 1 ratio of [DNA] : [Ru]. The Ru(II)-DNA solutions were allowed to incubate for 5 min before the absorption spectra were recorded. The intrinsic binding constant K_b of the Ru(II) complex to DNA was calculated based on equation (1) [29]:

$$(\varepsilon_a-\varepsilon_f)/(\varepsilon_b-\varepsilon_f)=(b-(b^2-2K_b^2C_t[\mathrm{DNA}]/s)^{1/2})/2K_bC_t, \quad (1a)$$

$$(b=1+K_bC_t+K_b[\mathrm{DNA}]/2s), \quad (1b)$$

where the apparent absorption coefficients ε_a, ε_f, and ε_b correspond to $A_{obsd}/[Ru]$, the absorbance for the free ruthenium complex, and the absorbance for the ruthenium complex in fully bound form, respectively. C_t is the total metal complex concentration and s is the binding site size (in base pairs).

The thermal denaturation was performed with a Perkin-Elmer Lambda 35 spectrophotometer equipped with a Peltier temperature-controlling programmer (±0.1°C). The melting curves were obtained by measuring the absorbance at 260 nm for solutions of CT-DNA (100 μmol L^{-1}) in the absence and presence of the Ru(II) complex (10 μmol L^{-1}) as a function of the temperature. The temperature of the solution was increased by 1°C min^{-1} and ramped from 50°C to 90°C. The data are presented as

$(A - A_0)/(A_f - A_0)$ *versus* temperature, where A, A_0, and A_f represent the observed, the initial, and the final absorbance at 260 nm, respectively.

The binding constant of the complex to CT-DNA at T_m was determined by equation (2) [30]:

$$\frac{1}{T_m^0} - \frac{1}{T_m} = \left(\frac{R}{\Delta H_m}\right) \ln(1 + K_b' L)^{1/n}, \tag{2}$$

where T_m^0 and T_m are the melting temperatures of CT-DNA alone and in the presence of the complex, respectively. ΔH_m is the enthalpy of DNA (per base pair), R is the gas constant, K_b' is the DNA-binding constant at T_m, L is the free Ru(II) complex concentration, and n is the binding site size.

The ΔH_m value of 6.9 kcal mol^{-1} (28.9 kJ mol^{-1}) was determined by differential scanning calorimetry [31]. According to van't Hoffs equations (3)–(5) [32], a series of thermodynamic functions can be calculated:

$$\ln\left(\frac{K_2}{K_1}\right) = \frac{\Delta H^0}{R}\left(\frac{1}{T_1} - \frac{1}{T_2}\right), \tag{3}$$

$$\Delta G_T^0 = -\mathrm{RT} \ln K, \tag{4}$$

$$\Delta G_T^0 = \Delta H - T\Delta S^0, \tag{5}$$

K_1 and K_2 are the DNA-binding constants of the complex at temperatures T_1 and T_2, respectively. ΔH^0, ΔG^0, and ΔS^0 are the changes in standard enthalpy, standard free energy, and standard entropy as the complex binds with CT-DNA.

Viscosity measurements were performed with an Ubbelodhe viscometer maintained at 30.0 ± 0.1°C in a thermostatic bath. DNA samples with an approximate average length of 200 base pairs were prepared by sonication in order to minimize complexities arising from DNA flexibility [33]. Flow time was measured with a digital stopwatch; each sample was measured three times, and an average flow time was calculated. Data are presented as $(\eta/\eta^0)^{1/3}$ *versus* binding ratio ([Ru]/[DNA]), where η is the viscosity of DNA in the presence of the complex and η^0 is the viscosity of DNA alone [34].

For the gel electrophoresis experiment, supercoiled pBR322 DNA (0.1 μg) was treated with the Ru(II) buffer solution, then irradiated at room temperature with a UV lamp (365 nm, 10 W). Samples were analyzed by electrophoresis after 1 h at 100 V on a 0.8% agarose gel in TBE (89 mmol L^{-1} Tris-borate acid, 2 mmol L^{-1} EDTA, pH = 8.3). The gel was stained with 1 μg mL^{-1} EB and photographed on an Alpha Innotech IS–5500 fluorescence chemiluminescence and visible imaging system.

2.5. *Scavenger measurements of hydroxyl radical (·OH)*

The hydroxyl radical (·OH) in aqueous media was generated by Fenton's reagent [35]. Solutions of the tested complexes were prepared with N,N-dimethylformamide (DMF) and 5 mL of assay mixture of safranin (28.5 μmol L^{-1}). EDTA-Fe(II) (100 μmol L^{-1}), H_2O_2 (44.0 μmol L^{-1}), the tested compounds (0.5–10.0 μmol L^{-1}), and a phosphate buffer (67 mmol L^{-1}, pH = 7.4) were prepared according to the literature method [36]. The assay mixtures were incubated at 37°C for 30 min in a water bath. The absorbance

was then measured at 520 nm. All the tests were run in triplicate and expressed as the mean. A_i was the absorbance in the presence of the tested compound; A_0 was the absorbance in the absence of the tested compound, A_c was the absorbance in the absence of the tested compound, EDTA-Fe(II), and H_2O_2. The suppression ratio (η_a) was calculated on the basis of $(A_i - A_0)/(A_c - A_0) \times 100\%$.

2.6. *Theoretical calculations*

The computations were made based on the structure (figure 1); all computations were performed with the G98 quantum chemistry program-package [37] at the DFT-B3LYP level [38–41] using the LanL2DZ basis set [42, 43]. The full geometric optimization computations for the ground states of Ru(II) complexes with the singlet state were carried out. In order to vividly depict the details of the frontier molecular orbital interactions, the stereographs of some related frontier molecular orbitals of the complexes were drawn using the Molden v3.7 program [44].

3. Results and discussion

3.1. *Crystal structure of 2*

Selected crystallographic data are given in table 1; selected bond lengths and angles are shown in table 2. Based on the X-ray structure of the cation of **2** (figure 2) and the data

Table 1. Crystal data and structural refinement for **2**.

Empirical formula	$C_{211}H_{192}Cl_8N_{32}O_{36}Ru_4$
Formula weight	4439.85
Temperature (K)	100(2)
Wavelength (Å)	0.71073
Crystal system	Triclinic
Space group	$P\bar{1}$
Unit cell dimensions (Å, °)	
a	14.7157(7)
b	15.0881(7)
c	23.3673(11)
α	75.9260(10)
β	78.3290(10)
γ	84.4100(10)
Volume (Å^3), Z	4922.1(4), 1
Calculated density (Mg m^{-3})	1.498
Absorption coefficient (mm^{-1})	0.494
$F(000)$	2282
Crystal size (mm^3)	$0.40 \times 0.25 \times 0.08$
θ range for data collection	1.48–25.50°
Index ranges	$-17 \le h \le 17$; $-18 \le k \le 18$; $-28 \le l \le 28$
Reflections collected/unique	36,771/18,068 [R(int) = 0.0362]
Completeness to $\theta = 25.50$ (%)	98.5
Refinement method	Full-matrix least-squares on F^2
Data/restraints/parameters	18,068/0/1282
Goodness-of-fit on F^2	1.017
Final R indices [$I > 2\sigma(I)$]	$R_1 = 0.0519$, $wR_2 = 0.1235$
R indices (all data)	$R_1 = 0.0789$, $wR_2 = 0.1335$
Largest difference peak and hole (e · Å^{-3})	0.856 and −0.854

in table 2, the Ru(II) center is octahedrally coordinated by six nitrogen atoms from two dmb ligands (N_1, N_2, N_3, and N_4) and one pdtp (N_5 and N_8), with an average intraligand bite angle of 78.50(12)° for N_a–Ru–N_a and 79.00(12)° for N_m–Ru–N_m (N_a and N_m denote nitrogen from dmb and pdtp, respectively). The mean bond lengths of Ru–N_a and Ru–N_m are 2.061(3) Å and 2.040(3) Å, respectively. The DFT computed and X-ray single-crystal diffraction experimental structure parameters are listed in table 3. The results indicate that the computed bond lengths, bond angles, and dihedral angles are in agreement with experimentally obtained parameters. The ligand pdtp in **2** has a larger aromatic planar area than that of pdpt in **1**.

3.2. *Electrochemical and electronic absorption properties*

The electrochemical potentials and cyclic voltammetry for **1** and **2** are given in table 4 and "Supplementary material". In the sweep range from −1.80 to 1.80 V (*vs.* SCE),

Table 2. Selected bond lengths (Å) and angles (°) for $[Ru(dmb)_2(pdtp)]^{2+}$.

Ru–N(1)	2.065(3)	Ru–N(2)	2.057(3)
Ru–N(3)	2.059(3)	Ru–N(4)	2.063(3)
Ru–N(5)	2.064(3)	Ru–N(8)	2.015(3)
N(2)–Ru–N(1)	78.02(12)	N(3)–Ru–N(4)	79.02(12)
N(8)–Ru–N(5)	79.24(12)	N(8)–Ru–N(4)	88.45(12)
N(2)–Ru–N(4)	173.92(12)	N(8)–Ru–N(3)	92.92(12)
N(8)–Ru–N(1)	173.57(12)	N(8)–Ru–N(2)	96.95(12)
N(3)–Ru–N(1)	91.75(12)	N(4)–Ru–N(1)	96.79(12)
N(2)–Ru–N(3)	97.85(12)	N(2)–Ru–N(5)	89.97(12)
N(3)–Ru–N(5)	169.58(12)	N(4)–Ru–N(5)	93.80(12)

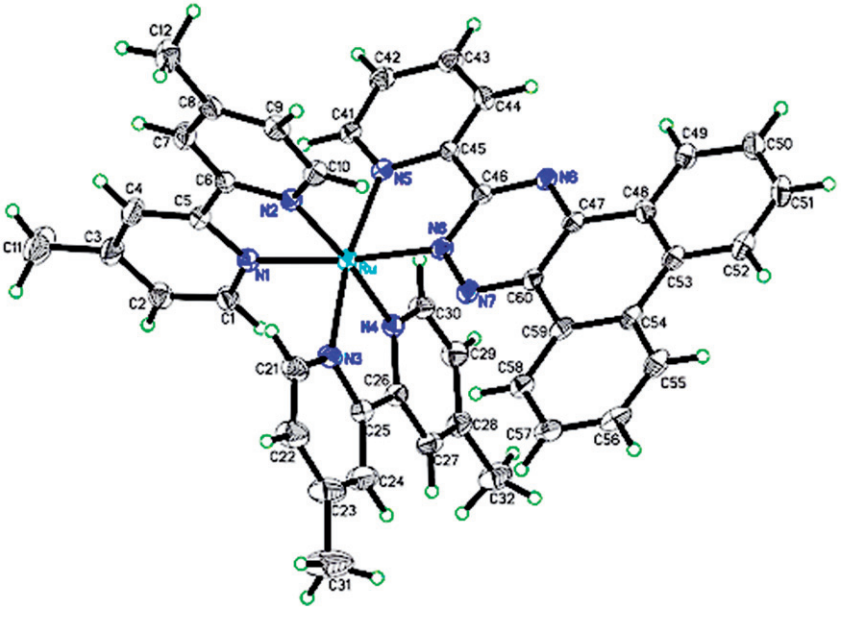

Figure 2. An ORTEP drawing of $[Ru(dmb)_2(pdtp)]^{2+}$ (50% probability level ellipsoids).

Table 3. DFT computed (Comp.) and X-ray diffraction experimental (Exp.) bond lengths (Å), bond angles. and dihedral angles (°) of **1** and **2**.

		$Ru–N_m$[a]	$Ru–N_a$[b]	$N_m–Ru–N_m$[c]	$N_a–Ru–N_a$[d]	Dihedral angle	
1	Comp.	2.087	2.097	78.4	78.3	29.1[e]	35.6[f]
2	Comp.	2.085	2.097	78.7	78.3	−0.3[e]	−0.8[f]
	Exp.	2.040	2.061	79.0	78.5	0[e]	0[f]

[a]$Ru–N_m$: mean bond length between Ru and coordination N atoms in pdpt or pdtp.
[b]$Ru–N_a$: mean bond length between Ru and coordination N atoms dmb.
[c]$N_m–Ru–N_m$: bond angle between coordination N atoms in pdpt or pdtp.
[d]$N_a–Ru–N_a$: mean bond angle between coordination N atoms in dmb; Dihedral angle: [e]N8–C9–C13–C14; [f]N11–C10–C24–C23.

Table 4. Redox potentials for the ruthenium(II) complexes, $E_{1/2}$[a] (V).

		Reduction		
Complex	Oxidation	i	ii	iii
1	1.26	−1.01	−1.56	−1.78
2	1.31	−0.80	−1.53	−1.72
[b]$[Ru(dmb)_3]^{2+}$	1.13	−1.37	−1.54	−1.80

[a]All complexes were measured in 0.1 mol L^{-1} NBu_4ClO_4–CH_3CN, $T = 25 \pm 1$°C, scan rate = 100 mV.
[b]Values taken from ref. [46].

both complexes show one oxidation wave corresponding to the Ru(III)/Ru(II) couple with peaks at 1.26 and 1.31 eV for **1** and **2**, respectively, and three successive reduction waves. The first reduction can be attributed to reduction of pdpt or pdtp, and the latter two successive reductions belong to dmb [19, 22, 45]. The reduction potentials of pdpt (−1.01 eV) and pdtp (−0.80 eV) are less negative than that of dmb (−1.37 eV) in $[Ru(dmb)_3]^{2+}$ [46], demonstrating that the triazine ring is electron-withdrawing, as in the case of some structurally related tridentate complexes [18].

Absorption spectra of the two complexes (figure 3) are characterized by intense π–π^* ligand transitions in the UV region of 240–360 nm, and metal-to-ligand charge transfer (MLCT) transitions in the visible region with peak at 493 and 480 nm for **1** and **2**, respectively [19].

According to the electron cloud distribution based on DFT calculation (figure 4) the HOMOs are mainly located on ruthenium showing a clear d_z2 shape, and the LUMOs are mostly located on the triazine rings of pdpt or pdtp. $E_{1/2}^{ox}$ and $E_{1/2}^{red}$ are relevant to the energies of HOMO and LUMO (listed in table 5), respectively. The oxidation potential of **2** (1.31 V) is higher than that of **1** (1.26 V), attributed to its lower energy HOMO (−10.443 eV) relative to that of **1** (−10.419 eV). That the half wave potential of the first reduction of **1** (−1.01 V) is more negative than that of **2** (−0.80 V) can be easily understood from the lower LUMO energy of **2** (−7.360 eV) than that of **1** (−7.344 eV). It is also interesting to correlate $\Delta E_{1/2}$ ($E_{1/2}^{ox} - E_{1/2}{}^{red}$) and the energy of MLCT (E_{MLCT}) to the energy difference between LUMO and HOMO as follows [21]:

$$\Delta E_{1/2}(\text{eV}) = (E_{LUMO} - E_{HOMO}) - 1.76,$$

$$E_{MLCT}(\text{eV}) = (E_{LUMO} - E_{HOMO}) - 0.67.$$

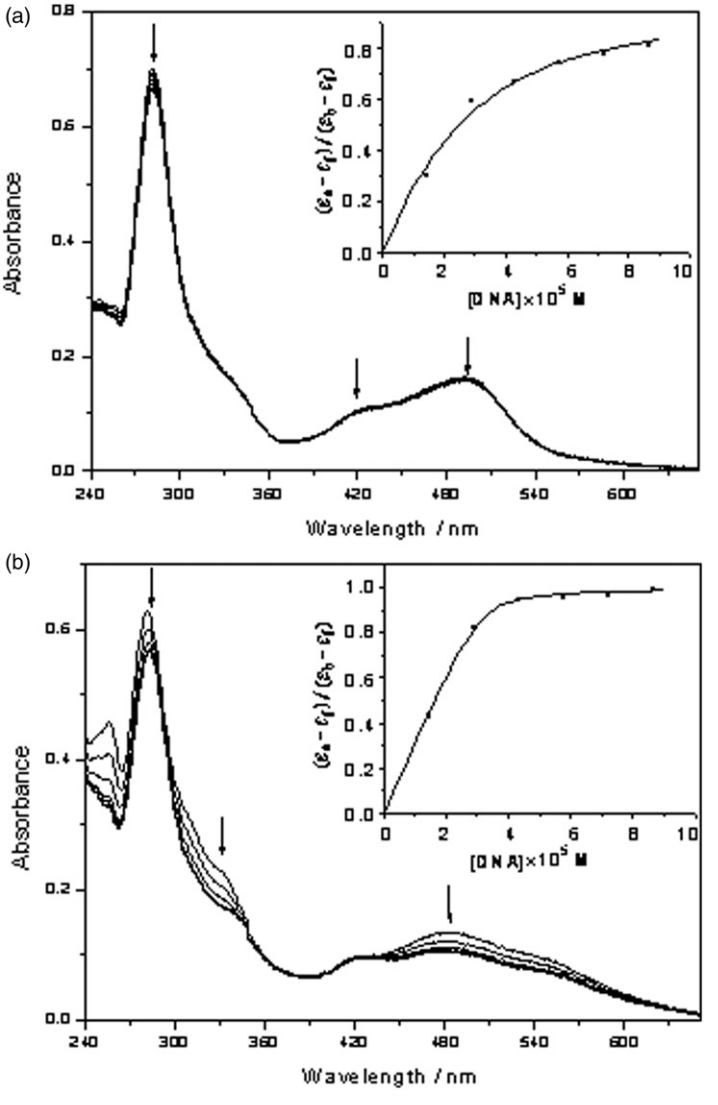

Figure 3. Absorption spectra of **1** (a) and **2** (b) in Tris-HCl buffer upon addition of CT-DNA ([Ru] = 12 μmol L^{-1}, [DNA] = 0–150 μmol L^{-1}). Arrows indicate the changes in absorbance with respect to increasing DNA concentration. Inset: plot of $(\varepsilon_a - \varepsilon_f) / (\varepsilon_b - \varepsilon_f)$ *vs.* [DNA] for titration of DNA to Ru(II) complexes.

All the computed values of E_{MLCT} and $\Delta E_{1/2}$ are in accord with the experimental values. The results are summarized in table 6.

3.3. *DNA-binding properties*

3.3.1. Electronic absorption titration. As shown in figure 3, with the addition of DNA, the MLCT charge transfer bands of **1** and **2** exhibit hypochromism of about 3.68% and

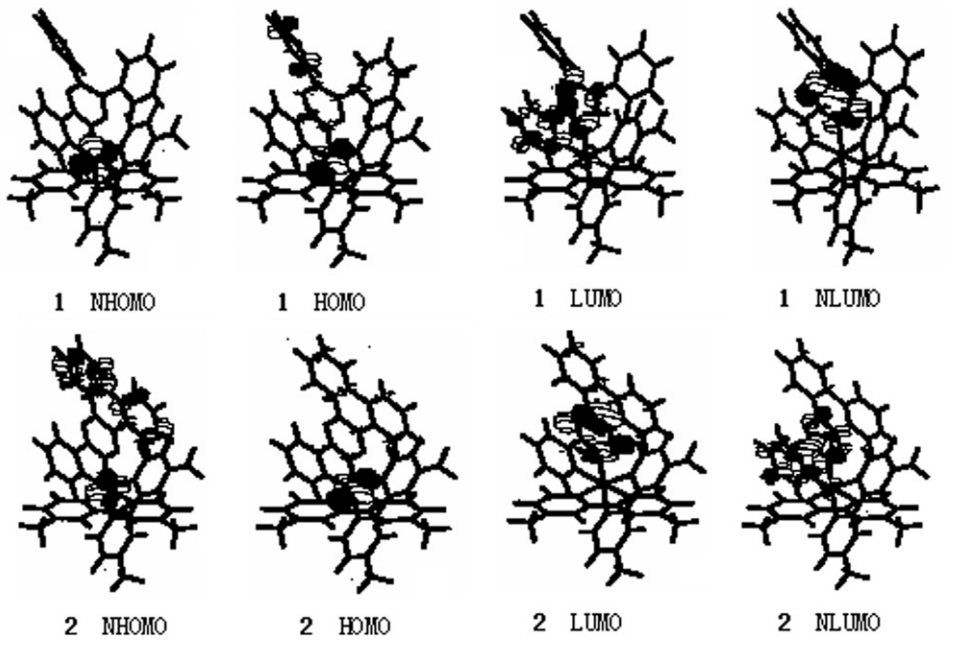

Figure 4. Some related frontier orbital stereographs of **1** and **2**. HOMO: highest occupied molecular orbital; NHOMO: next HOMO; LUMO: lowest occupied molecular orbital; NLUMO: next LUMO.

Table 5. Some frontier molecular orbital energies (E_i (eV)) of **1** and **2**.

	E_{NH}[a]	E_H[b]	E_{NL}[c]	E_L[d]	ΔE_{L-H}[e]
1	−10.563	−10.419	−7.140	−7.344	3.075
2	−10.538	−10.443	−7.260	−7.360	3.083

[a]E_{NH}: energy of next HOMO.
[b]E_H: energy of HOMO.
[c]E_{NL}: energy of next LUMO.
[d]E_L: energy of LUMO.
[e]ΔE_{L-H}: $E_L - E_H$.

Table 6. Experimental (Exp.) and computational (Comp.) values of E_{MLCT} and $\Delta E_{1/2}$ for **1** and **2**.

		1	**2**
E_{MLCT}	Exp.	493 nm	480 nm
	Comp.[a]	494 nm	484 nm
$\Delta E_{1/2}$	Exp.	2.27 eV	2.11 eV
	Comp.	2.31 eV	2.25 eV

[a]Unit conversion of eV to nm: 1 nm = 1240 per eV.

33.74%, and bathochromism of 3 and 4 nm, respectively. Here, the hypochromism of **1** is less than that of $[Ru(dmb)_2BFIP]^{2+}$ (14%, BFIP = 2-benzo[b]furan-2-yl-1H-imidazo[4,5-f][1,10]phenanthroline), but **2** is larger than $[Ru(dmb)_2BFIP]^{2+}$ [47]. The intrinsic constant K_b was obtained by fitting to equation (1) the changes of absorbance

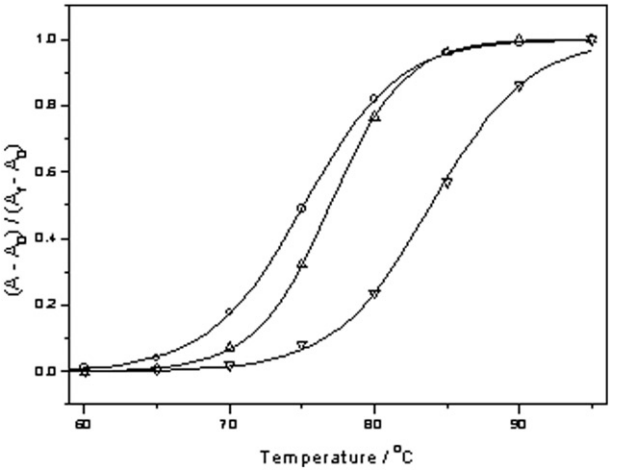

Figure 5. Melting temperature curves of DNA in the absence (o) and presence of **1** (Δ) and **2** (▽). [Ru] = 10 μmol L^{-1}, [DNA] = 100 μmol L^{-1}.

in the MLCT band with respect to increasing concentrations of DNA [29]. The resulting values of K_b are 6.9 ($\pm$0.4) $\times 10^4$ ($s = 0.51 \pm 0.02$) and 8.3 ($\pm$0.1) $\times 10^5$ $(\text{mol L}^{-1})^{-1}$ ($s = 1.47 \pm 0.02$) for **1** and **2**, respectively. The K_b of **2** is comparable to that of the reported aqueous soluble complex $[Ru(MeIm)_4(tip)]^{2+}$ ($K_b = 7.2 \times 10^5$ $(\text{mol L}^{-1})^{-1}$, MeIm = 1-methylimidazole, tip = 2-(thiophene-2-group)-1H-imidazo[4,5-f][1,10]phenanthroline) [48]. Here $s < 1$ (0.51) for **1** may result from its stacking each other onto the surface of the DNA. The result indicates that **2** has a larger DNA-binding affinity and DNA-binding constant K_b than **1**, because of a larger aromatic system area and lower energy of frontier molecular orbital LUMO.

3.3.2. Thermal denaturation studies. The melting curves of the absorption intensity at 260 nm of CT-DNA in the absence and presence of Ru(II) complexes *versus* temperature are given in figure 5. The CT-DNA melting point T_m alone is 75.1 $\pm$ 0.2°C under the given experimental conditions, and increases to 76.9 $\pm$ 0.2°C and 83.9 $\pm$ 0.2°C in the presence of **1** and **2**, respectively. Here T_m is defined as the temperature where half of the total base pairs is unbounded [1]. A series of thermodynamic functions denoted ΔH^0, ΔG^0, and ΔS^0 for DNA-binding of **1** and **2**, calculated with equations (2)–(5) are listed in table 7. The observed change of melting temperatures (ΔT_m) at a concentration ratio [DNA]/[Ru] = 10 : 1 are 1.8 and 8.8°C for **1** and **2**, respectively. The large increase in T_m of **2** is comparable to that of analogous complex $[Ru(dmb)_2(ITAP)](ClO_4)_2$ ($\Delta T_m = 6.7$°C, ITAP = isatino [1,2-b]-1,4,8,9-tetraazatriphenylene) [45]. Complex **2** binds to DNA *via* intercalation, and **1** binds in partial intercalation mode. Both the negative binding free energy and enthalpy suggest that binding of the complexes to DNA is energetically highly favorable at room temperature. The entropy change ΔS^0 of **1** (-77.9 J mol^{-1}) is more negative than that of **2** (-34.6 J mol^{-1}), further confirming stacking for **1** on the DNA surface, thus resulting in a greater decrease in entropy.

Table 7. Thermodynamic parameters based on DNA denaturation.

	1[b]	**2**[b]
T_m[a] (°C)	76.9	83.9
ΔT_m (°C)	1.8	8.8
K_b at T_m	3.2×10^3	4.4×10^4
K_b at 25°C	6.9×10^4 ($s = 0.51$)	8.3×10^5 ($s = 1.47$)
ΔG^{o}[c] (kJ mol^{-1})	−27.6	−33.8
ΔH^{o} (kJ mol^{-1})	−50.8	−44.1
ΔS^{o} (J mol^{-1})	−77.9	−34.6

[a]The T_m of CT–DNA alone was 75.1°C.
[b]The T_m of CT–DNA in the presence of Ru(II) complex in a 10 : 1 ratio of base pair to complex.
[c]The value of standard free energy change was set at 25°C.

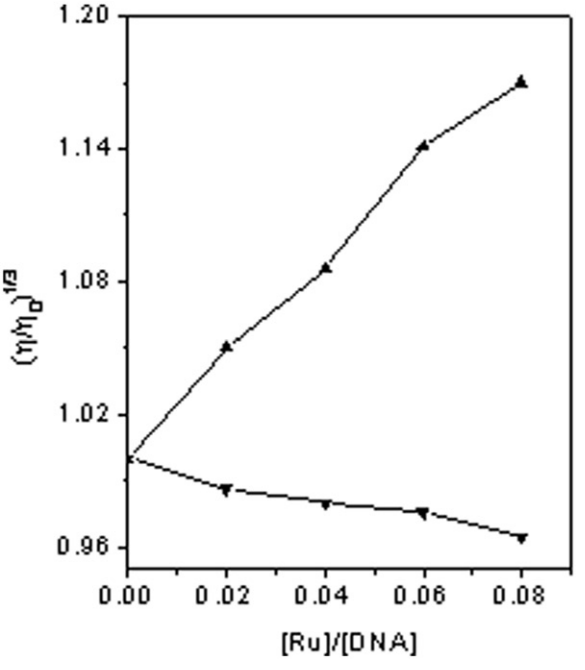

Figure 6. Effect of increasing amounts of **1** (▼) and **2** (▲) on the relative viscosities of DNA at 30.0 ± 0.1°C ([DNA] = 0.5 mmol L^{-1} and [Ru]/[DNA] = 0, 0.02, 0.04, 0.06, 0.08).

3.3.3. Viscosity measurements. Viscosity measurements for **1** and **2** are presented in figure 6. The relative viscosity of DNA decreases with increasing concentrations of **1**, whereas, when the amount of **2** is increased the relative viscosity of DNA increases steadily, confirming that the two complexes bind to DNA in different modes; **2** binds to DNA in a classical intercalation mode [19, 22, 49] while **1** binds to DNA in a partial intercalation mode [18].

3.4. *Photocleavage of pBR 322 DNA by Ru(II) complexes*

In gel electrophoresis, the moving rates of three types of circular plasmid DNA were different. The intact, supercoiled Form I was the fastest, the nicked Form II with one

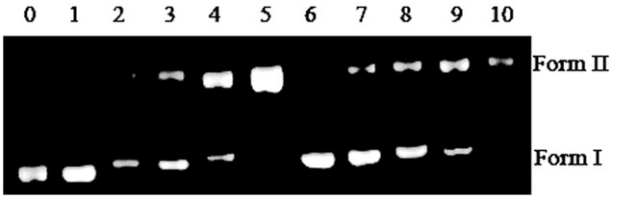

Figure 7. Photoactivated cleavage of pBR 322 DNA in the presence of different concentrations of **1** and **2** after irradiation at 365 nm for 30 min. Lane 0 (DNA alone), Lanes 1–5 for **1**: (1) 5 μmol L^{-1}, in dark, (2) 5 μmol L^{-1}, (3) 10 μmol L^{-1}, (4) 20 μmol L^{-1}, (5) 60 μmol L^{-1}. Lanes 6–10 for **2**: (6) 5 μmol L^{-1}, in dark, (7) 5 μmol L^{-1}, (8) 10 μmol L^{-1}, (9) 20 μmol L^{-1}, (10) 60 μmol L^{-1}.

cleaved strand was the slowest, and the linear Form III with both strands cleaved was between Form I and Form II [50].

The photocleavage of pBR 322 DNA, mediated by **1** and **2**, was monitored by agarose gel electrophoresis. The cleaving efficiencies of **1** and **2** are shown in figure 7. No obvious cleavage was observed when DNA alone was subjected to irradiation for up to 30 min at 365 nm, and when DNA was mixed with complexes in darkness for 30 min. With increasing concentration of **1** and **2**, the amount of intact supercoil form (Form I) pBR 322 DNA diminished gradually, whereas the nicked form (Form II) increased. At a concentration of 60 μmol L^{-1} for **1** and **2**, Form I was completely converted into Form II. It is important to note that, as discussed above, the partial side-on intercalation and stacking on the DNA surface that occurs for **1** can also give rise to DNA photocleavage.

3.5. *Antioxidant activity against the hydroxyl radical*

The Fenton system was used to produce the hydroxyl radical (•OH). The change in the amount of •OH with respect to an increase in the supply of Ru(II) complexes was determined by monitoring the absorbance intensity of safranin, which can be photobleached upon its reaction with •OH. This allows the antioxidant activity against the hydroxyl radical for **1** and **2** to be known. The curves of the scavenging ratio taken as $(A_i - A_0)/(A_c - A_0) \times 100\%$ *versus* the concentrations of **1** and **2** are presented in figure 8. The suppression of •OH by **1** and **2** reached 83.6% and 97.8% at 10 μmol L^{-1} of Ru(II) complexes, respectively.

The two Ru(II) complexes maintain efficient antioxidant activity against hydroxyl radical, and the scavenging ratio of **2** is much higher than that of **1** under the same experimental conditions, as shown in figure 8. The hydroxyl radical (•OH) is one of the most dangerous reactive oxygen species in the life of aerobic organisms. Its oxidation leads to DNA damage, and consequently causes diseases, such as cancer and chronic inflammation [51]. Both complexes show promise as potential antioxidants in therapeutic reagents.

4. Conclusion

Two new Ru(II) complexes, $[Ru(dmb)_2(pdpt)](ClO_4)_2$ (**1**) and $[Ru(dmb)_2(pdtp)](ClO_4)_2$ (**2**), have been synthesized and characterized. A series of experiments examining

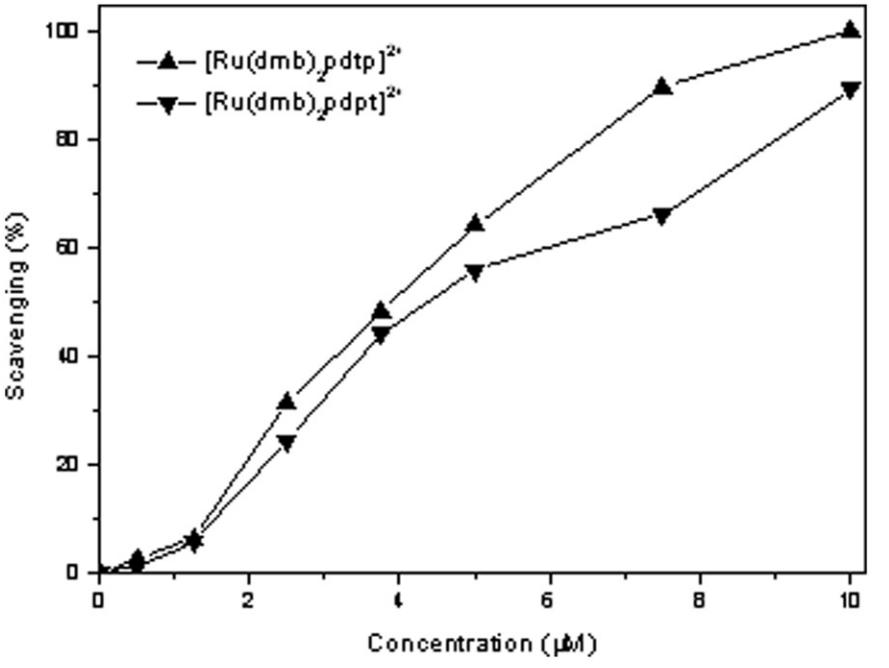

Figure 8. Scavenging effects of **1** and **2** on hydroxyl radicals. The concentrations of Ru(II) complexes are 0.5, 1.5, 2.5, 3.8, 5, 7.5, 10 μmol L^{-1}, respectively.

absorption titration, thermal denaturation, and viscosity measurement confirm that the DNA-binding affinity of **2** is much greater than that of **1**, and **2** binds to CT-DNA by intercalation, whereas **1** binds to CT-DNA in partial intercalation, with π–π stacking on the DNA surface. The trend in DNA-binding affinity, as well as certain electrochemical and spectral properties of the complexes, can be explained by DFT calculations. The two complexes effectively mediate photocleavage of pBR 322 DNA and maintain efficient antioxidant activity against the hydroxyl radical (•OH); these features, combined with their DNA-binding properties, suggest future use as components of anticancer drugs.

Supplementary material

Crystallographic data for the structure reported here have been deposited with the Cambridge Crystallographic Data Center (CCDC) as supplementary publication CCDC No. 790034. Copies of the data can be obtained free of charge on application to CCDC, 12 Union Road, Cambridge CB2 1EZ, UK (Fax: (+44) 1223-336-033; E-mail: deposit@ccdc.cam.ac.uk).

Acknowledgments

We are grateful to Shaoguan University for the financial support. We are indebted to Prof. K.C. Zheng (Sun Yat-sen University) for the good works on the DFT calculation,

and we are grateful to Prof. Chao Hui (Sun Yat-Sen University) for his specific directions.

References

[1] J.M. Kelly, A.B. Tossi, D.J. McConnell, C. OhUigin. *Nucleic Acids Res.*, **13**, 6017 (1985).
[2] A.E. Friedman, C.V. Kumar, N.J. Turro, J.K. Barton. *Nucleic Acids Res.*, **19**, 2595 (1991).
[3] L.N. Ji, X.H. Zou, J.G. Liu. *Coord. Chem. Rev.*, **216**, 513 (2001).
[4] F. Pierard, A.K.D. Mesmaekert. *Inorg. Chem. Commun.*, **9**, 111 (2006).
[5] H. Chao, F. Gao, L.N. Ji. *Prog. Chem.*, **19**, 1844 (2007).
[6] A.E. Friedman, J.C. Chambron, J.P. Sauvage, N.J. Turro, J.K. Barton. *J. Am. Chem. Soc.*, **112**, 4960 (1990).
[7] Y.J. Liu, C.H. Zeng, F.H. Wu, J.H. Yao, L.X. He, H.L. Huang. *J. Mol. Struct.*, **932**, 105 (2009).
[8] S. Shi, T.M. Yao, X.T. Geng, L.F. Jiang, J. Liu, Q.Y. Yang, L.N. Ji. *Chirality*, **21**, 276 (2009).
[9] B. Sun, Y.C. Wang, C. Qian, J. Chu, S.M. Liang, H. Chao, L.N. Ji. *J. Mol. Struct.*, **963**, 153 (2010).
[10] M.J. Clarke. *Coord. Chem. Rev.*, **236**, 209 (2003).
[11] A. Juris, V. Balzani, F. Barigelletti, S. Campagna, P. Belser, A.V. Zelewsky. *Coord. Chem. Rev.*, **84**, 85 (1988).
[12] Y. Jung, S.J. Lippard. *Chem. Rev.*, **107**, 1387 (2007).
[13] C.G. Hartinger, S. Zorbas-Seifried, M.A. Jakupec, B. Kynast, H. Zorbas, B.K. Keppler. *J. Inorg. Biochem.*, **100**, 891 (2006).
[14] U. Schatzschneider, J. Niesel, I. Ott, R. Gust, H. Alborzinia, S. Wolfl. *Chem. Med. Chem.*, **3**, 1104 (2008).
[15] S. Delaney, M. Pascaly, P.K. Bhattacharya, K. Han, J.K. Barton. *Inorg. Chem.*, **41**, 1966 (2002).
[16] Y.J. Liu, Z.H. Liang, Z.Z. Li, C.H. Zeng, J.H. Yao, H.L. Huang, F.H. Wu. *BioMetals*, **23**, 739 (2010).
[17] H.L. Huang, Y.J. Liu, C.H. Zeng, L.X. He, F.H. Wu. *DNA and Cell Biol.*, **29**, 261 (2010).
[18] X.L. Hong, H. Chao, L.J. Lin, K.C. Zheng, H. Li, X.L. Wang, F.C. Yun, L.N. Ji. *Helv. Chim. Acta*, **87**, 1180 (2004).
[19] X.L. Hong, H. Li, C.H. Peng. *J. Mol. Struct.*, **990**, 197 (2011).
[20] W.J. Frisch, Æ. Frisch, J.B. Foresman. *Gaussian 94 User's Reference*, Gaussian Inc., Pittsburgh, PA (1994–1995).
[21] S.R. Stoyanov, J.M. Villegas, D.P. Rillema. *Inorg. Chem.*, **41**, 2941 (2002).
[22] H. Deng, J. Li, K.C. Zheng, Y. Yang, H. Chao, L.N. Ji. *Inorg. Chim. Acta*, **358**, 3430 (2005).
[23] B.P. Sullivan, D.J. Salmon, T.J. Meyer. *Inorg. Chem.*, **17**, 3334 (1978).
[24] J. Marmur. *J. Mol. Biol.*, **3**, 208 (1961).
[25] M.E. Reichmann, S.A. Rice, C.A. Thomas, P. Doty. *J. Am. Chem. Soc.*, **76**, 3047 (1954).
[26] R.H. Blessing. *Acta Cryst.*, **A51**, 33 (1995).
[27] Bruker. *SHELXTL 5.1*, AXS, Madison, WI (1991).
[28] G.M. Sheldrick. *SHELX 97*, Göttingen University, Germany (1997).
[29] M.T. Carter, M. Rodriguez, A.J. Bard. *J. Am. Chem. Soc.*, **111**, 8901 (1989).
[30] J.D. McGhee. *Biopolymers*, **15**, 1345 (1976).
[31] S. Satyanarayana, J.C. Dabrowiak, J.B. Chaires. *Biochemistry*, **32**, 2573 (1993).
[32] H.Q. Liu, B.C. Tzeng, Y.S. You, S.M. Peng, H.L. Chan, M.S. Yang, C.M. Che. *Inorg. Chem.*, **41**, 3161 (2002).
[33] J.B. Chaires, N. Dattagupta, D.M. Crothers. *Biochemistry*, **21**, 3933 (1982).
[34] G. Cohen, H. Eisenberg. *Biopolymers*, **8**, 45 (1969).
[35] W.H. Koppenol. *Free Radical Biol. Med.*, **15**, 645 (1993).
[36] C.C. Winterbourn. *Biochem. J.*, **198**, 125 (1981).
[37] M.J. Frisch, G.W. Trucks, H.B. Schlegel, G.E. Scuseria, M.A. Robb, J.R. Cheeseman, V.G. Zakrzewski, J.A. Montgomery Jr, R.E. Stratmann, J.C. Burant, S. Dapprich, J.M. Millam, A.D. Daniels, K.N. Kudin, M.C. Strain, O. Farkas, J. Tomasi, V. Barone, M. Cossi, R. Cammi, B. Mennucci, C. Pomelli, C. Adamo, S. Clifford, J. Ochterski, G.A. Petersson, P.Y. Ayala, Q. Cui, K. Morokuma, N. Rega, P. Salvador, J.J. Dannenberg, D.K. Malick, A.D. Raghavachairi, J.B. Foresman, J. Cioslowski, J.V. Ortiz, A.G. Baboul, B.B. Stefanov, G. Liu, A. Liashenko, P. Piskorz, I. Komaromi, R. Gomperts, R.L. Martin, D.J. Fox, T. Keith, M.A. Al-Laham, C.Y. Peng, A. Nanayakkara, M. Challacombe, P.M.W. Gill, B. Johnson, W. Chen, M.W. Wong, J.L. Andres, C. Gonzalez, M. Head-Gordon, E.S. Replogle, J.A. Pople, *Gaussian 98, Revision A 11.4*, Gaussian, Inc., Pittsburgh PA (2002).
[38] P. Hohenberg, W. Kohn. *Phys. Rev. B*, **136**, 864 (1964).
[39] A.D. Becke. *J. Chem. Phys.*, **98**, 1372 (1993).
[40] A. Gorling. *Phys. Rev. A*, **54**, 3912 (1996).

[41] J.B. Foresman, E. Frisch. *Exploring Chemistry with Electronic Structure Methods*, 2nd Edn, Gaussian Inc., Pittsburgh, PA (1996).
[42] P.J. Hay, W.R. Wadt. *J. Chem. Phys.*, **82**, 270 (1985).
[43] W.R. Wadt, P.J. Hay. *J. Chem. Phys.*, **82**, 284 (1985).
[44] G. Schaftenaar, J.H. Noordik. *J. Comput. Aided Mol. Des.*, **14**, 123 (2000).
[45] F.H. Wu, C.H. Zeng, Y.J. Liu, X.Y. Guan, L.X. He. *J. Coord. Chem.*, **62**, 3512 (2009).
[46] N.H. Damrauer, T.R. Boussie, M. Devenney, J.K. McCusker. *J. Am. Chem. Soc.*, **119**, 8253 (1997).
[47] K.A. Kumar, K.L. Reddy, S. Satyanarayana. *J. Coord. Chem.*, **63**, 3676 (2010).
[48] X. Yang, Y. Liu, S. Yao, Y. Xia, Q. Li, W. Zheng, L. Chen, J. Liu. *J. Coord. Chem.*, **64**, 1491 (2011).
[49] J.G. Liu, Q.L. Zhang, X.F. Shi, L.N. Ji. *Inorg. Chem.*, **40**, 5045 (2001).
[50] H.Y. Mei, J.K. Barton. *Proc. Natl Acad. Sci. USA*, **85**, 1339 (1988).
[51] K. Tsai, T.G. Hsu, K.M. Hsu, H. Cheng, T.Y. Liu, C.F. Hsu, C.W. Kong. *Free Radical Biol. Med.*, **31**, 1465 (2001).